

Comparison of Combustion and Pollutant Emission Models for DI Diesel Engines

G. D'Errico, D. Ettore, T. Lucchini

Politecnico di Milano, Dipartimento di Energetica - Milano, Italy

Copyright © 2007 Society of Automotive Engineers, Inc.

ABSTRACT

The increasing interest in the Diesel engine technology and the continuous demand of reducing fuel consumption and emissions has motivated over the years the development of advanced numerical models, to provide qualitatively predictive tools for the designers (injection strategy, flow optimization, EGR level, combustion and emission control) and investigation tools for the researchers to complement optical diagnostics. Nevertheless, there is not a common agreement about many fundamental phenomena which have been extensively investigated (turbulence-chemistry and flame-wall interactions, pollutant formation, very lean and very rich combustion) and each model has been implemented into different codes and validated with respect to different operating conditions.

In this work two significant approaches with different level of complexity for Diesel combustion modelling have been analyzed and implemented by the authors in the same opensource code, OpenFOAM: the Eddy Dissipation model and the PaSR (Partially Stirred Reactor) model. For what regard the latter, the potentialities and accuracy of the ISAT (In-Situ Adaptive Tabulation) algorithm, recently implemented by the authors into OpenFOAM, to reduce significantly the required computational time were evaluated. Similarly, different models to predict pollutant emissions are revised and tested, due to considering the need to fulfil the future emission regulations imposing further reductions in NO_x and soot.

The mentioned models were applied to simulate a selection of significant Constant-Volume Diesel Combustion test-cases from the Engine Combustion Network database [1]. These data are particularly worth of interest since they have a public domain access,

providing a framework for collaborative comparisons, and they include detailed information about pressure rise, liquid penetration length, ignition delay, lift-off length and soot distribution. The selected and simulated conditions consider n-heptane as fuel and include different oxygen concentrations and thermodynamic states (ambient density and temperature). Finally a real engine configuration was considered and the obtained results were compared against cylinder pressure data and pollutant concentrations.

INTRODUCTION

The development and assessment of a CFD methodology and its implementation into a numerical simulation toolkit specifically tailored for engine simulation represents a very challenging task. In particular Diesel engine modelling requires to describe into details many simultaneous interacting thermofluids and chemical processes, which take place in a domain with a complex geometry and moving boundaries. On the modelling front, the task is to assemble a complete and accurate description of the involved physical process, while on the numerical viewpoint, the challenge is the development of flexible and efficient algorithms with respect to the implementation of the model equations and to the description of the engine geometry [2]. The objective to aim at is the definition of a reliable CFD code which can be used as a predictive tool from a qualitative viewpoint in a design stage and as a diagnostic tool to achieve a deeper understanding of the occurring physical phenomena. Within this context, in recent works [3, 4] Reitz et al. compared three different Diesel combustion models, all implemented into a modified version of the KIVA-3V code, underlying the importance of unique CFD tool to be used to simulate identical conditions by means of different approaches. Similarly, Venugopal and

Abraham [5] extensively reviewed different approaches to model flame lift-off, showing how at the moment none of the available models may be completely adequate, but any simulation result is obviously dependent on the code implementation and case set-up. However the implementation of a new model by a sequential programming language is extremely time consuming, requiring significant modifications in numerous parts of the code.

The last and less obvious challenge to CFD simulation is the availability of suitable experimental data to guide the development and assess the accuracy of the proposed models [2]. In this field, a significant contribution is represented by the Engine Combustion Network database [3], which aims at establishing “an internet library of well-documented experiments that are appropriate for model validation and the advancement of scientific understanding of combustion at conditions specific to engines”.

On the basis of the above mentioned considerations, the authors intend to contribute to develop a CFD platform for the simulation of internal combustion engines, whose fundamental prerequisites are the following:

- to be written in an highly efficient object-oriented programming to allow an easy implementation and testing of new models;
- to be opensource to allow collaborative studies regarding both the model implementation and validation (any CFD result often depends on several parameters whose set-up should be of public domain for model assessment).

To these ends, the authors have contributed over the last years to the development and application of the multi-purpose CFD code *OpenFOAM* [6, 7]. In this paper, the state of the art of the code regarding Diesel engine modelling is discussed, including recent enhancement introduced by the authors, and an initial comparison among combustion and emission models of different complexity, applied to simulate a selection of available Sandia vessel measurements [1] and some operating points of a commercial Diesel engine.

In the following sections a brief overview of the adopted physical models to describe Diesel spray evolution, combustion and emission formation is given, discussing in some detail the different approaches to model the turbulence-chemistry interaction and the soot formation. Successively the class definition to model Diesel combustion is presented, to illustrate the advantages of object orientation when complex and interacting physical models need to be implemented.

DIESEL SPRAY MODEL

The Eulerian-Lagrangian approach is used [8, 9] to model the fuel-air mixture formation in direct-injection engines. To calculate the evolution of the spray into the

gaseous atmosphere, two phases need to be described: the dispersed liquid and the continuous gas phase, which interact each other according to their exchanges of mass, momentum and energy. The gas phase is described using the Navier-Stokes equations, while the Lagrangian formulation describes the evolution of the multi-component liquid phase. The spray is represented by points, often referred to as *parcels*. These points are then assigned properties which may be as many as desired, like location, velocity, diameter and fuel composition [9, 10]. Different sub-models are then used to describe liquid fuel injection, primary and secondary breakup, droplet evaporation, heat-exchange, collisions and turbulent dispersion.

OpenFOAM has been recently used for Lagrangian spray modelling and further details about experimental validations and implementation can be found in [9, 11, 12, 13]. The code already includes most of the widely used sub-models for spray breakup, fuel injection, droplet collisions, evaporation and turbulent dispersion. In this work, a constant spray angle is assumed, while the initial droplet diameter is derived by the injector diameter and its area contraction coefficient [9]. Both the Kelvin-Helmoltz and Rayleigh-Taylor mechanisms are accounted for to model the spray breakup [14]. The Ranz-Marshall correlation [15] is used to model the droplet evaporation. Droplet to droplet interactions and turbulence dispersion effects are neglected. The reader is also referred to [9] for further details.

COMBUSTION MODELS

The two different combustion models evaluated in this work will be now presented. The first one is based on the Eddy Dissipation Model and it can be used as a development tool since its limited computational demand. The second one is the Partially Stirred Reactor Combustion model [16] and uses complex chemistry to model ignition and mixed-controlled combustion. For these reasons, it requires higher computational time than the first approach and is more suitable for diagnostic purposes. However, it provides a better insight of the combustion process taking place during the ignition and combustion phases. For both the approaches, the RNG $k - \varepsilon$ is used to model turbulence as suggested in [4, 9].

MODIFIED EDDY DISSIPATION MODEL

In Diesel engine combustion, the fuel is injected into the hot, compressed air and auto-ignition plays an important role in the combustion and flame stabilization processes. After ignition, combustion is generally mixing-controlled [17]. For these reasons, the fuel reaction rate can be expressed as:

$$\bar{\omega}_F = (1 - \alpha)\bar{\omega}_{F,ign} + \alpha\bar{\omega}_{F,mix} \quad (1)$$

where α is used to switch from the auto-ignition ($\alpha = 0$) to the mixing-controlled combustion mode ($\alpha = 1$). Expressions for both $\bar{\omega}_{F,ign}$ and $\bar{\omega}_{F,mix}$ are thus required.

Auto-ignition: When the fresh gases are ignited, all the fuel contained in a computational cell is burned. Hence $\bar{\omega}_{F,ign}$ is equal to:

$$\bar{\omega}_{F,ign} = \tilde{Y}_F / \Delta t \quad (2)$$

where \tilde{Y}_F is the fuel mass fraction and Δt is the computational time-step at the ignition time. Following the approach of Pires De la Cruz [18], a self-ignition progress variable Y_I monitors how close the fresh gases are from igniting. The average value of the progress variable is transported through convection and diffusion inside the combustion chamber according to the equation:

$$\frac{\partial \bar{\rho} \tilde{Y}_I}{\partial t} + \frac{\partial}{\partial x_i} (\bar{\rho} \tilde{u}_i \tilde{Y}_I) = \frac{\partial}{\partial x_i} \left(\bar{\rho} D_t \frac{\partial \tilde{Y}_I}{\partial x_i} \right) + \bar{\omega}_I \quad (3)$$

The rate of growth of the progress variable \tilde{Y}_I is proportional to the amount of the fuel tracer $\tilde{Y}_{T,fu}$ in the mixed zone and is a function of the local self-ignition delay, which depends on the fresh gas thermodynamic conditions. The fuel tracer represents the amount of fresh mixed fuel that would exist in the computational cell in absence of chemical reactions. It is a passive scalar because, by definition, it is neither consumed nor created by chemical reactions.

The rate of growth of \tilde{Y}_I is equal to [18]:

$$\bar{\omega}_I = \bar{\rho} \tilde{Y}_{T,Fu} F(\tau_d) \quad (4)$$

which is valid until $\tilde{Y}_I < \tilde{Y}_{T,Fu}$. From the definition of the progress variable, the self-ignition delay τ_d in the preceding conditions is given by:

$$\int_0^{\tau_d} F(\tau_d) = 1 \quad (5)$$

$F(\tau_d)$ is defined as:

$$F(\tau_d) = \frac{1}{\tau_d} \quad (6)$$

τ_d represents the ignition delay as a function of the local thermodynamic conditions in each cell (pressure, temperature, air/fuel ratio, ...).

The ignition delay in the computational cell is reached when $\tilde{Y}_I \geq \tilde{Y}_{T,Fu}$. After ignition, the fuel burns according to the Equation 2 and α is set to one since the combustion becomes mixing-controlled.

The ignition delay τ_d is estimated according to an Arrhenius correlation [19]:

$$\tau_d = A p^{-n} \exp(E_a / RT) \quad (7)$$

The Eddy Dissipation Model (EDM) by Magnussen and Mjergarter [20] estimates the mixing-controlled fuel burning rate $\bar{\omega}_{F,mix}$ from fuel (\tilde{Y}_F), oxidizer (\tilde{Y}_O) and product mean mass fractions (\tilde{Y}_P) and depends on the

turbulent mixing time, estimated from integral length scales as $\tau_t = k/\varepsilon$:

$$\bar{\rho} \bar{\omega}_{F,mix} = C_{mag} \bar{\rho} \frac{\varepsilon}{k} \min \left(\tilde{Y}_F, \frac{\tilde{Y}_O}{s}, \beta \frac{\tilde{Y}_P}{(1+s)} \right) \quad (8)$$

where C_{mag} and β are two model constants. In Equation 8, the reaction rate is limited by the deficient mean specie. When β is finite, this deficient species may be combustion products to take into account the existence of burnt gases, providing the energy required to ignite fresh reactants.

Coupling the Eddy Dissipation Model for mixing-controlled combustion with an ignition treatment makes it possible to predict both ignition and flame stabilization since fuel and oxidizer do not immediately ignite as soon as they meet [17].

PARTIALLY STIRRED REACTOR MODEL

Chomiak, Golovichev et al. [16, 21, 22] applied detailed kinetics and the Partially Stirred Reactor concept (PaSR) to correctly describe the turbulence/chemistry interaction in Diesel spray combustion.

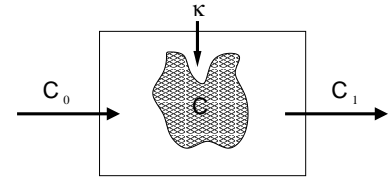


Figure 1: Conceptual picture of the Partially Stirred Reactor.

In the PaSR approach, a computational cell is split into two different zones: in one zone all reactions occur, while in the other one there are no reactions. Thus, the composition changes due to mass exchange with the reacting zone. Furthermore, the reacting zone is treated as a Perfectly Stirred Reactor (PSR), in which the composition is homogeneous. According to the PaSR concept, the concentration of each species i at the exit of reactor can be defined as:

$$c_1^i = \kappa^* c^i + (1 - \kappa^*) c_0^i \quad (9)$$

where κ^* is the mass fraction of the mixture which reacts. As shown in Figure 1, the model distinguishes between three molar concentrations:

- c_0^i is the averaged concentration in the feed of the cell and may be considered as the initial averaged concentration in the cell;
- c^i is the unknown concentration in the reaction zone on a sub-grid level in the unknown reactive fraction of the cell material;
- c_1^i is the sought for, time-averaged exit concentration. This is also the averaged concentration in the cell;

According to Equation (9), c_1^i is a linear interpolation between c^i and c_0^i and the whole combustion process can be split in two sub-steps, proceeding in parallel (see also Figure 2):

- 1) The initial concentration in the reaction zone changes from c_0^i to c^i ;
- 2) The reactive mixture c^i is mixed by turbulence with c_0^i resulting in the averaged concentration c_1^i .

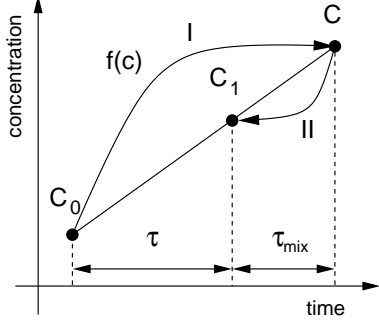


Figure 2: The reaction/mixing step procedure.

Since c_1^i is the initial value for the next time-step, the time between c_0^i and c_1^i must be the integration step, τ . The turbulence mixes c with c_0^i , hence the time difference between c^i and c_1^i must be the characteristic time for turbulence, τ_{mix} . Assuming that the slope of the curve in Figure 2 is equal to the reaction rate in the reaction zone, it results:

$$\frac{c_1^i - c_0^i}{\tau} = \frac{c^i - c_0^i}{\tau_{mix}} = f(c^i); \quad \kappa^* = \frac{\tau}{\tau + \tau_{mix}} \quad (10)$$

$f(c^i)$ is the reaction rate of the species i during the time-step τ which is calculated according to Equation 21. To obtain c_1 , it is now necessary to eliminate c in Equation 9. Using the Taylor expansion, the term $f(c^i)$ can be expressed as:

$$f(c^i) = f(c_1^i) + \left. \frac{\partial f}{\partial c} \right|_{c=c_1^i} (c^i - c_1^i) \quad (11)$$

The term $\frac{\partial f}{\partial c}$ is assumed to be the reciprocal of a chemical time scale:

$$\frac{1}{\tau_c} = -\frac{\partial f}{c_r} \quad (12)$$

and is calculated in this work as:

$$\left. \frac{\partial f}{\partial c} \right|_{c=c_1^i} = \frac{\dot{\omega}(c_1^i) - \dot{\omega}(c_0^i)}{c_1^i - c_0^i} \quad (13)$$

where $\dot{\omega}(c_1^i)$ and $\dot{\omega}(c_0^i)$ are the reaction rate expressions of the species i calculated at the beginning and at the end of the time step. Thus, Equation 11 becomes:

$$f(c^i) = f(c_1^i) - \frac{c^i - c_1^i}{\tau_c} \quad (14)$$

Substituting the expression of τ_c in Equation 9 the following expression is finally obtained for the sub-grid reaction rate:

$$\frac{c_1^i - c_0^i}{\tau} = \frac{\tau_c}{\tau_c + \tau_{mix}} f_m(c_1^i). \quad (15)$$

The reactive fraction κ_i becomes equal to:

$$\kappa_i = \frac{\tau_c}{\tau_c + \tau_{mix}} \quad (16)$$

Several expressions were proposed for the mixing time τ_{mix} [16, 22]. In this work, it is assumed to be proportional to a geometric mean of the Taylor and Kolmogorov times:

$$\tau_{mix} = C_{mix} \sqrt{\tau_t \tau_k} \quad (17)$$

where C_{mix} is a tuning constant.

For each chemical species, the following transport equation, containing the turbulence-chemistry interaction has to be solved:

$$\frac{\partial \bar{\rho} \tilde{Y}_i}{\partial t} + \frac{\partial}{\partial x_i} (\bar{\rho} \tilde{u}_i \tilde{Y}_i) = \frac{\partial}{\partial x_i} \left(\bar{\rho} D_t \frac{\partial \tilde{Y}_i}{\partial x_i} \right) + \kappa_i \bar{\omega}_i \quad (18)$$

$i = 1, \dots, N_{sp}$

where $\bar{\omega}_i$ is equal to $f(c_1^i)$ and represents the reaction rate of the species according to the used kinetic mechanism; N_{sp} is the number of chemical species involved.

IN-SITU ADAPTIVE TABULATION (ISAT)

The PaSR concept introduces the complex chemistry in the specie transport equation. This increases significantly the computational time, in fact the CFD time-step is much larger than the chemical one and for this reason it is appropriate to employ an operator-splitting approach where the change in composition resulting from the CFD timestep is evaluated separately from the contributions of advection and diffusion, and to subcycle the chemistry over the CFD timestep. An ODE stiff solver integrates the array of the compositions \mathbf{C} over the CFD time-step as a function of their reaction rate S :

$$\mathbf{C}(t_0 + \Delta t) = \mathbf{C}_0(t_0) + \int_{t_0}^{t_0 + \Delta t} S(\mathbf{C}, T, p) dt'. \quad (19)$$

The reaction mapping $\mathbf{R}(C_0)$ is thus defined as:

$$\mathbf{R}(C_0) = \mathbf{C}_0(t_0) + \int_{t_0}^{t_0 + \Delta t} S(\mathbf{C}, T, p) dt'. \quad (20)$$

The chemical source term in Equation 18 is then determined as follows:

$$\bar{\omega}_i = \frac{\mathbf{C}(t_0 + \Delta t) - \mathbf{C}_0(t_0)}{\Delta t} \quad (21)$$

To correctly calculate $\bar{\omega}_i$, a system of N_p stiff and non-linear differential equations should be solved for each cell at each time-step. At present, the existing computational

techniques and computer memory limitations prohibit implementation of fully detailed description of combustion chemistry into CFD simulation of complex flow patterns.

Several approaches based on tabulation of the reaction rates were proposed in the past to significantly reduce the computational time [18, 23] by using tabulated reaction-rates. However, the exploration of chemical look-up tables which take into account more than two or three coordinates may become prohibitive in terms of computational costs (memory access and multilinear interpolations). On the other hand, only a very small part of the table is generally used during the simulation since only a small part of the composition space is accessed. To overcome these difficulties, Pope and Young [24, 25] propose to build the chemical table as needed on-the-fly during the computation (*in situ*).

Each table entry contains the thermochemical composition (C_0, T, p) , the reaction mapping $\mathbf{R}(C_0)$ and the mapping gradient $\mathbf{A}(C_0) = (\partial R_i(C) / \partial c_i)$ measures the sensitivity of the reaction mapping to changes in composition and provides the coefficients required for linear interpolations. The entry is complemented with the size of the region of accuracy where a reaction mapping may be estimated from this entry by a linear interpolation with an error below a tolerance ϵ_{tol} assigned by the user. When the reaction mapping $\mathbf{R}(C^q)$ is required for a query composition C^q , the closest composition C^0 in the table is first determined through a binary tree, whose structure is shown in Figure 3.

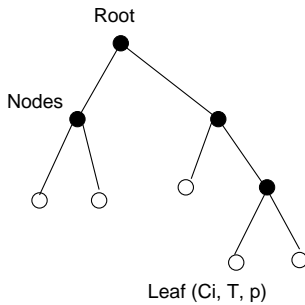


Figure 3: Binary Tree used to store the tabulated thermochemical states.

Three actions are then possible:

- If C^q lies in the region of accuracy of the existing table entry C^0 , a simple linear interpolation is performed (*retrieve*).

$$\mathbf{R}(C^q) = \mathbf{R}(C^0) + \mathbf{A}(C^0)(C^q - C^0) \quad (22)$$

- If C^q is outside the region of accuracy of the table entry C^0 , $\mathbf{R}(C^q)$ is determined by integration of Equation 19 and is compared to the linear interpolation of Equation 22, providing the corresponding error ϵ . Two cases are then considered:

- If the error ϵ is lower than the tolerance ϵ_{tol} prescribed by the user, the size of the region of accuracy of the table entry C^0 is increased (*growth*).
- If the error ϵ is larger than ϵ_{tol} , a new table entry is generated (*addition*).

The ISAT algorithm has been successfully applied to the simulation of steady combustion systems, where the speed-up obtained can be of the order of 1000 with respect to direct integration [26]. Recent application of ISAT for IC engine simulations are reported in [27], where a speed-up higher than 10 is generally obtained for each time-step. This is mainly caused by the drastic changes in temperature, pressure and compositions taking place during the combustion process, causing a continuous growth of the database. However, the obtained speed-up can be considered acceptable.

In the present work, the constant approximation has been used for the reaction mapping, thus the mapping gradient matrix is set to zero to reduce the computational time and the memory overheads. This approach has also been followed in other works applying the ISAT algorithm to engine simulations [27].

PREDICTION OF POLLUTANT EMISSIONS

SOOT EMISSIONS

The processes of soot formation and its subsequent burnout present particular challenges to computationally based flow-field prediction in a wide range of practical combustion systems. Even if the details of the physical and chemical processes are now understood, severe constraints imposed by the required computational time and available memory, limit the complexity of the models which can be used. For this reason, simplified phenomenological models are generally used, constructed around a small number of variables which are characteristic of the sooting process (for example soot volume fraction (f_v) and number density (N_p)). The two different phenomenological models compared in this work will be now presented.

Hiroyasu Model This is the most commonly used model for soot emission prediction in Diesel engines [3, 8, 28]. It considers two competing processes: soot formation and oxidation. The rate of change of the soot mass \dot{M}_s within a computational cell is determined from the soot formation rate \dot{M}_{sf} and soot oxidation rate \dot{M}_{so} .

$$\frac{dM_s}{dt} = \frac{dM_{sf}}{dt} - \frac{dM_{so}}{dt} \quad (23)$$

The formation rate uses an Arrhenius expression:

$$\frac{dM_{sf}}{dt} = A_{sf} M_{sp} P^n \exp\left(-\frac{E_{sf}}{RT}\right) \quad (24)$$

where A_{sf} is a tuning constant, M_{sp} is the mass of the soot inception species (C_2H_2 or fuel), P is the pressure and T is the temperature.

The soot oxidation rate uses the Nagle-Strickland Constable [29] formulation:

$$\frac{dM_{so}}{dt} = \frac{6MW_C}{\rho_s D_s} M_s R_{tot} \quad (25)$$

Expressions for R_{tot} can be found in [8].

When detailed chemistry is used, fuel is depleted quickly to form intermediate hydrocarbon species once reactions start [3, 4]. Thus, it is no longer useful to use fuel as the inception species for soot formation. Therefore, based on the previous literature and available species in the reaction mechanism used in this study, it was decided to use acetylene C_2H_2 as the inception species for soot formation, i.e., $M_{C_2H_2}$ in Equation 24. This is because acetylene is the most relevant specie pertaining to soot formation in hydrocarbon fuels. The pre-exponential constant A_{sf} was adjusted accordingly for the present implementation and also to account for the fuel effects.

Moss Model The phenomenological model by Moss [30] is based on the simplified representations of the processes of nucleation, heterogeneous surface growth, coagulation and oxidation as they apply to the balance between transport and production of soot volume fraction f_v and particle number density n . The respective source terms take the forms:

$$\frac{d}{dt} (\rho_s f_v) = \gamma n + \delta - \left(\frac{36\pi}{\rho_s} \right)^{1/3} n^{1/3} (\rho_s f_v)^{2/3} R_{tot} \quad (26)$$

$$\frac{d}{dt} (n/N_0) = \alpha - \beta (N/n_0)^2 \quad (27)$$

α and β are nucleation and coagulation rates, while γ and δ represent the impact of surface growth and nucleation on the soot volume fraction. The reader is referred to [30, 3] for further details about the expressions for the reaction rates.

NO_x EMISSIONS

Two different models to predict NO_x emissions have been evaluated. The first one is integrated into the Eddy Dissipation Model and estimates the formation rate of NO according to the simplified reaction rate [8], based on the first reaction of the Zel'dovich mechanism and it evaluates the oxygen concentration from partial equilibrium assumptions [31].

When the PaSR model is used, the chemistry of NO is part of the detailed kinetic scheme. The mechanism considers 9 reactions, and the NO_x emissions are the sum of NO and NO_2 emissions. This approach for NO_x emissions has also been used by Reitz and co-authors in [3, 4].

NUMERICAL CODE

Over the years, great emphasis has been given to the definition of mathematical models to describe the occurring phenomena and many fundamental aspects still require further studies. In the previous sections, a representative range of physical approaches required to achieve Diesel engine modelling have been discussed. Nevertheless the high complexity of the models and the existing interrelations make the numerical solution methodology play a role of equal importance as the mathematical modelling.

Discretisation accuracy, solver efficiency, geometry-handling capabilities and computer implementation are the paramount numerical requirements [2]. In this section the methodology used in OpenFOAM in last two named with regard to Diesel engine modelling is discussed.

MESH MANAGEMENT

The OpenFOAM code supports polyhedral cells of arbitrary shapes and for this reason it can be used for the simulation of complex geometries like internal combustion engines where moving boundaries such as piston and valves are present. In a recent work [32], the authors implemented into the OpenFOAM code a novel automatic-mesh motion technique with integrated topological changes, to keep the optimum mesh size and high quality during the whole simulation and to avoid the significant pre-processing manual work required for mesh motion. Most of Diesel engine CFD simulations considers only the compression and combustion phases on a sector of the combustion chamber. In this case mesh motion is accommodated in two different ways:

- *Dynamic layering*: Far from the TDC, layers of cells are added or removed close to the piston surface to keep the optimum mesh size, this is particularly useful in the case of the simulation of pilot injections happening 30-50 deg BTDC;
- *Mesh deformation*: The grid is deformed around the TDC to keep the number of cells at minimum and increase the mesh resolution when combustion and the main injection occur.

OBJECT-ORIENTED MODELLING OF DIESEL SPRAY COMBUSTION

An Eulerian frame model is generally represented as a set of coupled partial differential equations with the terms falling into several categories (the temporal derivative, convective and diffusive transport and various source and sink terms). Its implementation is generally a difficult and challenging subject, since it requires not only detailed knowledge of the physics and numerics but also of the software in which the model is implemented. Consequently model implementation may lead to possible coding errors, making testing and maintenance extremely

time consuming. Focusing the attention on Diesel engine simulation, code implementation should account for several fundamental issues, such as:

- The spray and the pressure field must know all the properties of the mesh (cells, volumes, boundaries);
- The spray parcels evolve according to the gas pressure and temperature fields, but these two fields should not be modified when the Lagrangian particles are moved;
- In the implementation of the mass, momentum and energy equations, the spray source terms are required;
- New spray sub-models should be introduced without modifying other parts of the code (solvers, mesh, . . .);

An object-oriented framework allows the software designer to create a more manageable software, with lower maintenance cost, extensive code re-use, fewer bugs and easier extendibility. The leading object-oriented language today is C++ [33, 34]: it provides not only the support for object orientation and generic programming but also offers near-universal availability and efficiency needed for scientific computations. The main features of the language are *data abstraction*, allowing the designer to introduce new data types appropriate for the problem, *object orientation*, (bundling of data and operations into classes, protecting the data from accidental corruption and the creating class hierarchies), *operator overloading*, which provides natural syntax for newly defined classes and generic programming, allowing code re-use for equivalent operations on different types.

For what concerns the present work, modelling of Diesel engines involves the following objects in OpenFOAM:

- the *engineTime* object contains all the control parameters for the simulation and the engine geometry data;
- the *engineMesh* object represents a polyhedral mesh with mesh motion and topological changes;
- the *dieselSpray* class is the Lagrangian description of the fuel spray. Basically it is a list of points in the mesh with properties like temperature, diameter, velocity, position, The *spray* class includes other objects representing the sub-models (*breakupModel*, *atomizationModel*, *evaporationModel*, . . .). All the spray sub-models are run-time selectable.
- different *scalarFields* represent the thermo-chemical state of the system (pressure, temperature, composition, enthalpy, . . .);
- a *vectorField* represents the velocity;
- a *turbulenceModel* which can be run-time selectable ($k - \epsilon$, RNG $k - \epsilon$, Low-Re $k - \epsilon$, . . .), providing to the transport equations the turbulent viscosity and thermal diffusivity;

- *sootModel*: run-time selectable model to predict soot emissions (Moss or Hiroyasu);
- Matrices and their algebra (*fvMatrix*);
- Numerical methods for temporal and spatial discretizations (*ddtScheme*, *divScheme*, *laplacianScheme*);

The model-to-model interaction is dealt by constant or non-constant access to protect the object data and functions. For example the *spray* class knows the pressure and velocity field, but cannot modify it. The interaction between the liquid and the gas phase is dealt by a series of functions in the *spray* class, representing the mass, momentum and energy source terms. In this way, only the top-level solver becomes a sequence of operations performed on each involved object .

Finally, the code is tailored to represent the models. As an example, the implementation of the Equation 18 in the code is:

```
solve
(
    fvm::ddt(rho, Yi)
    + fvm::div(phi, Yi)
    - fvm::laplacian(turbulence->muEff, Yi)
==
    dieselSpray.evaporationSource(i)
    + kappa*chemistry.RR(i)
)
```

If this is accomplished, the model structure, its implementation and inter-equation coupling could be examined independently from the related numerical issues. Further details about object-oriented programming applied to CFD modelling can be also found in [7, 35]

EXPERIMENTAL VALIDATION

Experimental data coming from an optically accessible vessel [36, 37] were used to validate the discussed combustion and emission models and their code implementation. After that, the different models were applied to simulate the combustion processes in a direct-injection, turbocharged engine for automotive applications.

SANDIA COMBUSTION CHAMBER

The SANDIA vessel is an optically accessible, constant-volume combustion chamber. It has a cubical shape, with a centrally mounted common-rail injector. After burning a specified premixed mixture before the start of injection, it is possible to reproduce high pressure and temperature environments similar to those found in Diesel engines at the injection time. Experimental data of vessel pressure, flame lift-off and soot distribution were used to validate the proposed combustion models. The chosen injection pressure was 150 MPa with a top-hat profile and the

injected fuel was n-heptane. A wide range of experimental conditions is available in the database, the ones used for the present validation are reported in Table 1.

| Case | 1 | 2 | 3 | 4 |
|--|------|------|------|------|
| Ambient density [kg/m^3] | 14.8 | 14.8 | 30 | 14.8 |
| O_2 volume fraction [%] | 21 | 15 | 15 | 21 |
| Ambient temperature [K] | 1000 | 1000 | 1000 | 1300 |

Table 1: Selection of experimental conditions tested for the SANDIA combustion vessel case.

The used computational grid represents a quarter of the real combustion chamber and has about 22000 cells, with radial and axial resolutions of 2 mm. The wall temperature was adjusted in each case to match the experimental cool-down pressure-profile [1].

The model constants for the EDM and the PaSR model are shown in Figure 2.

| | |
|------|--------------------------|
| EDM | $C_{mag} = 4; \beta = 1$ |
| PaSR | $C_{mix} = 0.005$ |

Table 2: Model constants used in the present work for the PaSR and the EDM combustion models.

Figures 4-5 show the flame evolution computed by the two combustion models for the case 1. The stoichiometric line is evidenced in black, while the white line evidences the 1600 K iso-line. 3 ms after the start of injection, the flame can be considered fully developed. The two combustion models predict a rather different flame structure. In the PaSR model, ignition occurs in a small, lean premixed region at the side of the vapor jet. Then, the flame propagates both upstream and downstream along the stoichiometric surface with very different velocities. The typical triple flame structure can be recognized when the flame is stabilized. The flame structure computed applying the implemented PaSR model agrees with the results obtained by Chomiak and Karlsson in [21].

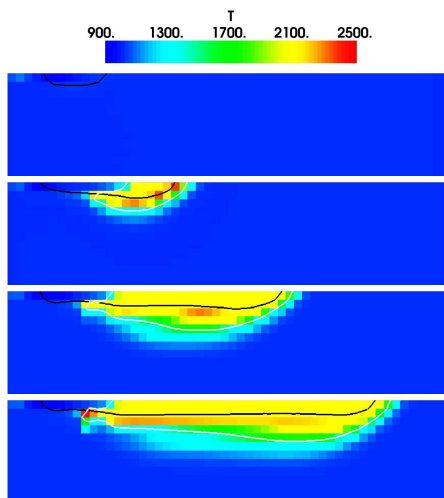


Figure 4: Computed flame evolution predicted by the PaSR model (0.5 ms, 1 ms, 2 ms, 3 ms).

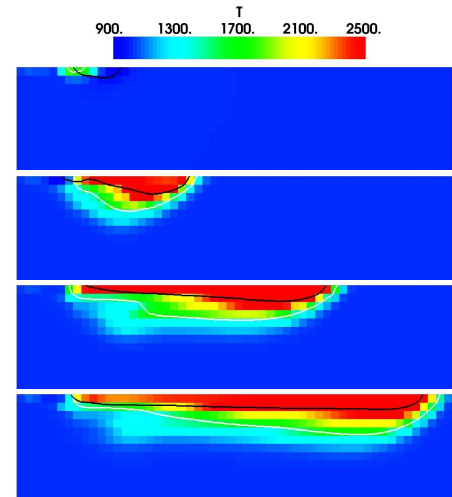


Figure 5: Computed flame evolution predicted by the EDM model (0.5 ms, 1 ms, 2 ms, 3 ms).

In the EDM model, the fuel ignites along the injector axis, and then the flame propagation is governed by mixing and turbulence, according to Equation 8. This is not in agreement with experimental findings [38] but it is related to the chosen correlation for ignition-delay, which is not a function of the equivalence ratio and ignition takes place where the mixture is rich. As a consequence, the computed lift-off is much lower than the one predicted by the PaSR approach.

A comparison between the experimental and the computed pressure rates is displayed in Figure 6 for all the tested cases. Premixed combustion is evidenced by the high peak in the pressure rate soon after the ignition, then mixing-controlled combustion takes place with a constant pressure rate which decreases to zero after the end of the fuel injection. The prediction of the ignition delay is strongly influenced by the chosen approach. In particular, the Wolfer correlation seems to match very well the cases 1-3, where the initial temperature is 1000 K, where complex chemistry overestimates the ignition time delay. This can be directly connected to the used kinetic scheme [39], since the same trend has been obtained also considering each cell as a Perfectly Stirred Reactor neglecting the influence of the turbulence, as discussed in [40]. The pressure rise during the mixing-controlled combustion is correctly predicted by both models, even if the PaSR approach slightly underestimates it in the case 4. Other investigations are required with different kinetic schemes to better understand the PaSR behavior during the auto-ignition phase.

Table 3 compares the experimental and predicted flame lift-off. In the calculations, the flame lift-off height was identified by a 1600 K temperature iso-line. The lift-off values computed by the EDM model are underestimated in all the cases. This is mainly due to the predicted ignition location, which is along the injector axis and very close to the injector. Considering the axial cell

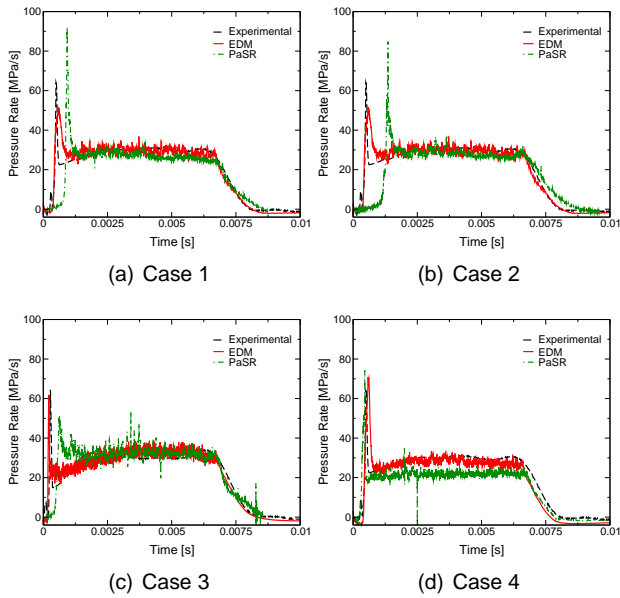


Figure 6: Experimental and computed pressure rates.

resolution of 2 mm, the PaSR model results are in good agreement with the experimental data, except the case 3, where the computed value is strongly influenced by the wrong prediction of the ignition delay. Furthermore, the PaSR correctly reproduces the experimental decrease in flame lift-off when the ambient temperature or the ambient density are increased.

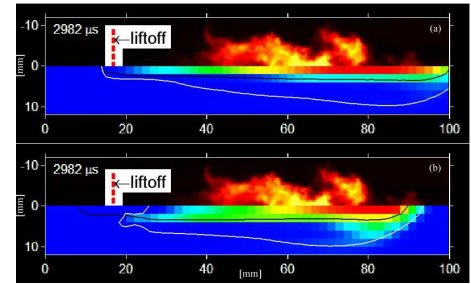
| Case | 1 | 2 | 3 | 4 |
|----------------------|----|------|------|-----|
| Experimental [mm] | 17 | 23.4 | 11.9 | 7.7 |
| Computed (EDM) [mm] | 8 | 8 | 6.7 | 5 |
| Computed (PaSR) [mm] | 18 | 40 | 10.0 | 6 |

Table 3: Experimental and computed flame lift-off values for the four cases.

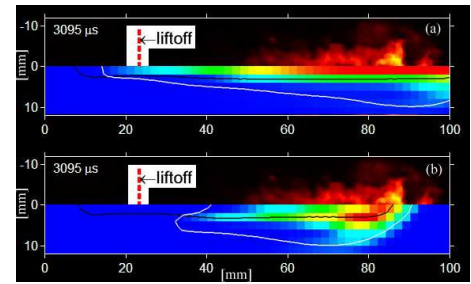
Finally, soot luminosity images are qualitatively compared with the soot concentrations computed by the two combustion models. Note that it was observed [36, 37] that the spatial locations of soot in PLII images closely coincide with features in the luminosity images, suggesting that the luminosity is due primarily to natural incandescence from hot soot. In each case shown in Figures 7(a)-(d), the upper image compares the EDM results with the experimental soot luminosity, while the lower refers to the PaSR results. All fields are shown at 3 ms, a time which is within the quasi-steady period. The computed stoichiometric and 1600 K temperature isolines are also reported as well as the experimental lift-off lengths.

The soot distribution is influenced by the flame temperature and the precursor concentration. The EDM model predicts high soot concentrations only very close to the injector axis, where the mixture is rich and the consequent fuel concentration is high. The PaSR model predictions agrees better than the EDM ones with the experimental data. However, the peak soot emission location is overestimated by both models in the first and fourth case, where the oxygen concentration is 21%. For

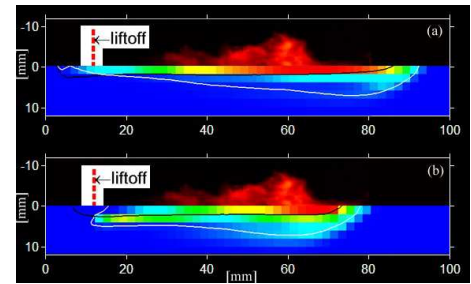
the other two cases with an initial concentration of O_2 of 15%, the PaSR predictions are in rather well agreement with experimental data and the model seems to correctly reproduce experimental variation in the peak soot region when the ambient density is increased [37], even if in the case 2 the flame lift-off is not correctly predicted.



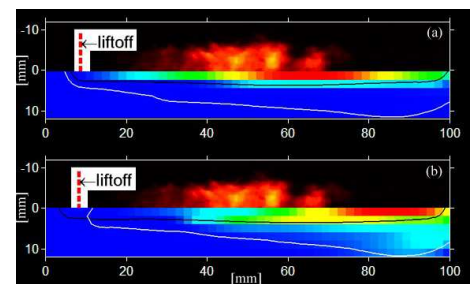
(a) Case 1



(b) Case 2



(c) Case 3



(d) Case 4

Figure 7: Computed soot fields and experimental soot PLII distributions. The experimental lift-off length is also shown in the pictures for each case.

ENGINE SIMULATIONS

A FIAT 1.2L engine, HSDI, four valve, common rail, multi-jet, turbocharged unit, whose main characteristics are listed in Table 4, was modelled.

| | |
|---------------------------------------|----------------------------------|
| Engine Type | HSDI 4-S Diesel |
| Number of cylinder | 4 in-line |
| Total displacement [cm ³] | 1248 |
| Bore [mm] | 69.6 |
| Stroke [mm] | 82 |
| Con. rod length [mm] | 131.3 |
| Compression ratio | 17.6:1 |
| IVC | -147° BTDC |
| Numebr of valves per cylinder | 4 |
| Air Metering | VGT turbocharger, Intercooler |
| Injection System | Common Rail, Multi-Jet |
| Max. Injection Pressure [MPa] | 160 |
| Injector hole diameter [mm] | 0.121 |
| Number of injector Holes | 6 |
| Spray angle | 155° |

Table 4: Main specifications of the HSDI turbocharged Diesel engine investigated

An experimental campaign was carried out on this engine at the dynamometer bench, at both full and partial loads [41]. Six engine speeds with different injection strategies were simulated and they are summarized in Figure 8. These six operating conditions are representative of six modes of Diesel combustion with three different injection strategies and SOI at full load, and three different EGR concentrations at partial load. The purpose is to have a significant range of cases, characterized by dominant premixed combustion or mixing-controlled combustion.

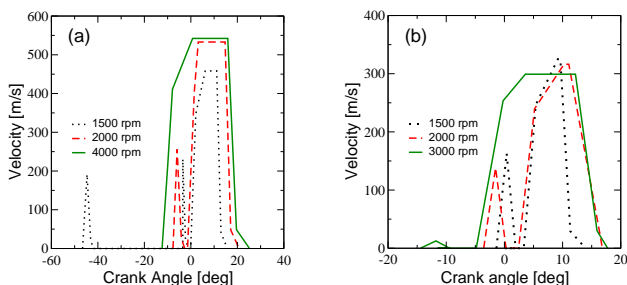


Figure 8: Fuel injection strategies [41]. (a) Full load; (b) Partial load.

The computational grid used for the simulations is shown in Figure 9; a 60° sector mesh was used in this study, considering that the Diesel injector has six equally-spaced nozzle holes. The block-structured mesh is composed of hexahedra and counted about 20000 computational cells, at bottom dead center (BDC), with 2x1x2.5 mm cell size in the bowl. The mesh was created using the OpenFOAM *blockMesh* utility, elements are added and removed, adapting automatically the mesh to the piston movement, in order to keep a roughly constant mesh resolution. The initial amount of swirl in the incoming air is accounted with a Bessel function profile for the air velocity within the combustion chamber. For all cases, calculations start at the intake valve closure (IVC). Initial thermodynamic conditions (pressure, temperature and

EGR) were deduced by a 1-D simulation of the whole engine system [41]. An example of pressure trace

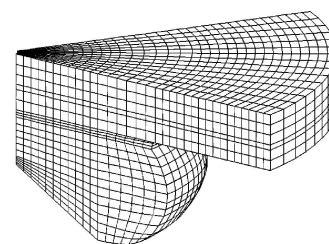


Figure 9: Computational grid at 20 CA BTDC.

comparison between computed values and experimental data is shown in Figure 10 (4000 rpm, full load). The PaSR approach predicts well the peak-pressure, but overestimates the ignition delay. The Wolfer correlation used in the EDM model provides a better estimation of the auto-ignition time.

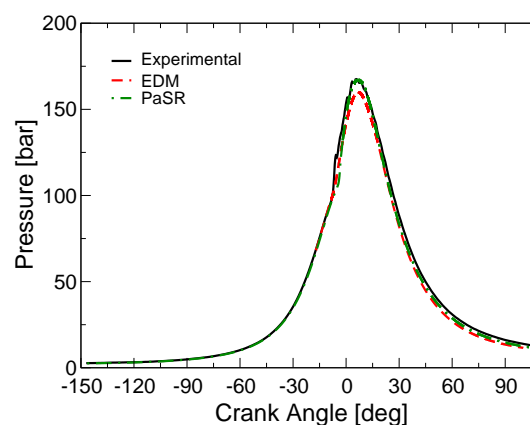


Figure 10: In cylinder pressure: full load - 4000 rpm

Figures 11 and 12 compare the computed NO_x and soot concentrations at the exhaust valve opening timing with the measured values, as a function of the engine speed at full and partial loads. The PaSR model, which includes a detailed description of chemical kinetics, has the capability to predict rather well the nitrogen oxides concentrations, both in terms of trend and absolute values at full load. Discrepancies characterize the part load comparison, even if the absolute values are very low. Note that the absence of experimental data of pressure and heat release at partial load did not allow any comparison. The PaSR approach with the Moss model and C₂H₂ as a precursor, captures better the trend of normalized soot than the Hiroyasu model with fuel as a precursor, both at full and partial load. Finally, much poorer results were obtained by the EDM approach, due to the fact that it includes only one global reaction for NO_x and soot.

The flame structure is displayed in Figures 13 and 14

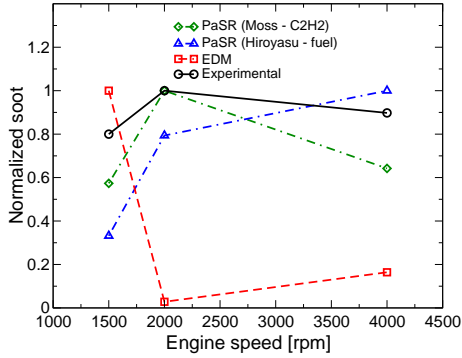
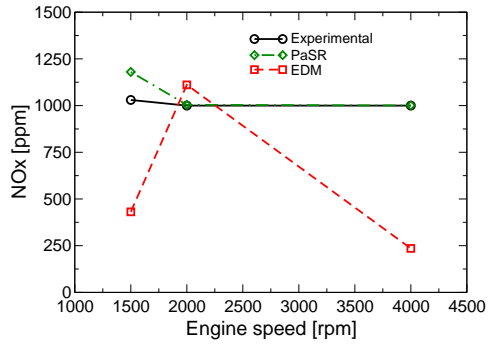


Figure 11: Comparison between predicted and measured NO and soot emission as a function of engine speed at full load.

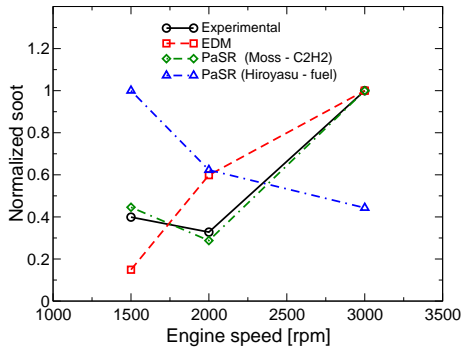
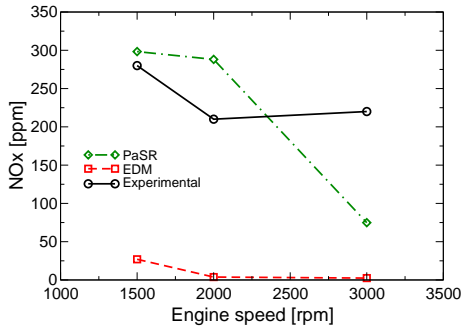


Figure 12: Comparison between predicted and measured NO and soot emission as a function of engine speed at partial load.

where the cell temperature is plotted at -3° and 2° ATDC on a horizontal and a vertical plane. In both cases, there is an inhomogeneous, cleft flame shape as shown by the high temperature white iso-line. The different ignition locations and soot distributions (Figures 15 and 16) can be appreciated.

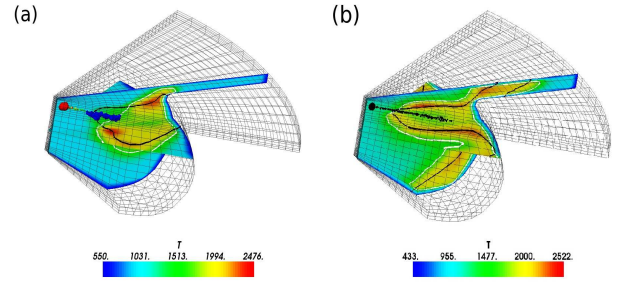


Figure 13: Flame structure with the PaSR model at: (a) 2° BTDC; (b) 3° ATDC (full load, 4000 rpm)

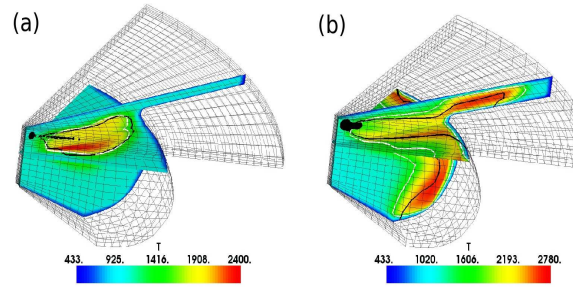


Figure 14: Flame structure with the EDM model at: (a) 2° BTDC; (b) 3° ATDC (full load, 4000 rpm)

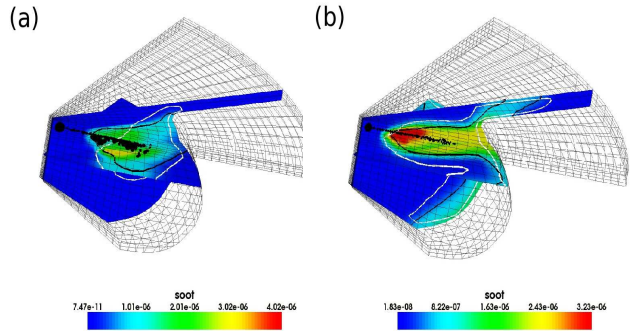


Figure 15: Soot distribution with the PaSR model at: (a) 2° BTDC; (b) 3° ATDC (full load, 4000 rpm)

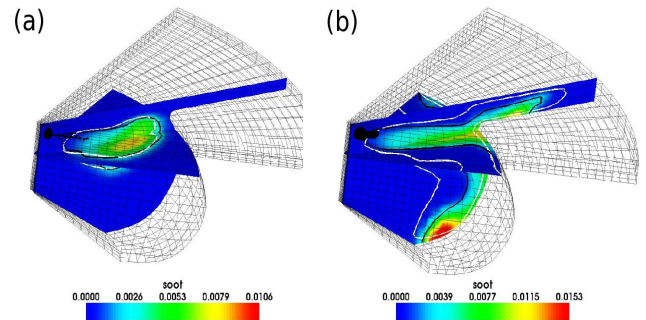


Figure 16: Soot distribution with the EDM model at: (a) 2° BTDC; (b) 3° ATDC (full load, 4000 rpm)

Finally a consideration about the CPU time performance required by the different approaches is due. The simulations were performed on a AMD 64 3GHz processor and the elapsed calculation time are shown

in Table 5. Note that also the comparison between the calculation time with ISAT versus a direct integration of the complex chemistry is shown. A tolerance of 10^{-4} was used in the ISAT control parameters and allowed a speed-up factor equal to 6.

| Model | Elapsed Time |
|-----------------------------|--------------|
| Complex chemistry with DI | 170 [h] |
| Complex chemistry with ISAT | 30 [h] |
| EDM | 3 [h] |

Table 5: Computational time required by the different approaches.

CONCLUSIONS

In this work, a CFD open-source platform has been further developed by the authors to evaluate different models for Diesel combustion. In particular two combustion models were implemented: the Eddy Dissipation Model (EDM) and the Partially Stirred Reactor (PaSR) model. The EDM model was modified to account for the effect of the ignition-delay; the PaSR model accounts for the turbulence-chemistry interaction when complex chemistry is used. In this case, to reduce the computational time, the In-Situ Adaptive Tabulation algorithm by Pope [42] was implemented by the authors.

Validation was performed with experimental data of a combustion vessel and a direct-injection turbocharger diesel engine for automotive applications. Both combustion models seem to correctly represent the pressure rate trend in the SANDIA combustion vessel and in the Fiat engine. This is rather encouraging for the EDM model whose computational time is very low. However, the simplified approach chosen to compute the ignition delay influences the predicted flame structure; the effect of tabulated ignition delays approaches, as proposed by De La Cruz [18], will be evaluated in a future work. The flame predicted by the authors' implementation of the PaSR model resembles the results by Chomiak and Karlsson [21], but further investigations on this model are still required: experiments and DNS calculations show that the ignition takes place on the rich side [38, 43]. This can also be the cause of an overestimation of the ignition delay observed in all the studied cases. The use of complex chemistry can also improve the soot emission capabilities by using a semi-empirical model.

The choice of an object-oriented code has also allowed an easy implementation of the combustion and pollutant emission models and offers great possibilities for future developments of the present work.

ACKNOWLEDGEMENTS

The financial support of Advanced Marine Power Technology SEATEK S.P.A. is gratefully acknowledged. The authors are also grateful to Mr. Gilles Hardy and Mr. Mario Mazuran for the interesting suggestions

provided during this work and to the the Msc students Valentina Contini and Paolo Ferrario for their contribution in the implementation of the Eddy Dissipation Model into OpenFOAM.

References

- [1] SANDIA Engine Combustion Network Database. <http://www.ca.sandia.gov/ecn>, 2006.
- [2] A. D. Gosman. State of the Art of Multi-Dimensional Modeling of Engine Reacting Flows. *Oil and Gas Science and Technology*, 54(no. 2), 1999.
- [3] S. Singh, R. D. Reitz, and M. P. B. Musculus. Comparison of the Characteristic Time (CTC), Representative Interactive Flamelet (RIF), and Direct Integration with Detailed Chemistry Combustion Models against Optical Diagnostic Data for Multi-Mode Combustion in a Heavy-Duty DI Diesel Engine. *SAE Paper*, 2006-01-0055, 2006.
- [4] S.C. Kong, Y. Sun, and R. D. Reitz. Modeling Diesel Spray Flame Liftoff, Sooting Tendency, and NO_x Emissions Using Detailed Chemistry With Phenomenological Soot Model. *Journal of Engineering for Gas Turbines and Power*, 129:pp. 245–251, 2007.
- [5] R. Venugopal and J. Abraham. A Review of Fundamental Studies Relevant to Flame Lift-off in Diesel Jets. *SAE Paper*, 2007-01-0134, 2007.
- [6] OpenFOAM website. <http://www.openfoam.org>. OpenCFD Limited, 2007.
- [7] H.G. Weller, G. Tabor, H. Jasak, and C. Fureby. A Tensorial Approach to CFD using Object Orientated Techniques. *Computers in Physics*, Vol. 12(No. 6):620, 1998.
- [8] G. Stiesch. *Modeling Engine Spray and Combustion Processes*. Springer, 2003.
- [9] N. Nordin. *Complex Chemistry Modeling of Diesel Spray Combustion*. PhD thesis, Chalmers University of Technology, Department of Thermo Fluid Dynamics, 2001.
- [10] A. D. Gosman and D. Clerides. Diesel Spray Modelling: A Review. *ILASS Europe Annual Meeting*, 1997.
- [11] T. Lucchini, G. D'Errico, and N. Nordin. CFD Modeling of Gasoline Sprays. *SAE Paper*, 2005-24-86, 2005.
- [12] H. Jasak, H.G. Weller, and N. Nordin. In-Cylinder CFD Simulation Using a C++ Object-Oriented Toolkit. *SAE Paper*, 2004-01-0110, 2004.
- [13] F. P. Karrholm and N. Nordin. Numerical Investigation of Mesh/Turbulence/Spray Interaction for Diesel Applications. *SAE Paper*, 2005-01-2115, 2005.
- [14] R. D. Reitz. Modeling Atomization Processes In High Pressure Vaporizing Sprays. *Atomization and Spray Technology*, Vol. 3:pp. 309–337, 1987.
- [15] C. Crowe, M. Sommerfield, and Y. Tsuji. *Multiphase Flows with Droplets and Particles*. CRC Press LLC, 1998.

- [16] V. Golovichev, N. Nordin, R. Jarnicki, and J. Chomiak. 3-D Diesel Spray Simulations Using a New Detailed Chemistry Turbulent Combustion Model. *SAE Paper*, 2000-01-1891, 2000.
- [17] T. Poinso and D. Veynante. *Theoretical and Numerical Combustion*. Edwards, 2005.
- [18] A. Pires De La Cruz. Modeling Diesel Spray Flame Liftoff, Sooting Tendency, and NO_x Emissions Using Detailed Chemistry With Phenomenological Soot Model. *Combustion Science and Technology*, 176:pp. 867–887, 2004.
- [19] H. H. Wolfer. Ignition Lag in Diesel Engines. *VDI-Forschungsheft*, 392, 1938.
- [20] B. F. Magnussen and B. H. Mjertager. On Mathematical Modelling of Turbulent Combustion. *Proceedings of 16th Symposium (International) on Combustion*, pages 719–727, 1976.
- [21] J. Chomiak and A. Karlsson. Flame Liftoff in Diesel Spray. *Proceedings of the Twenty-Sixth Combustion Symposium (International)*, pages pp. 2557–2564, 1996.
- [22] J. Kusaka, N. Horie, Y. Daisho, V. Golovichev, and S. Nakayama. Numerical Simulation Accounting for the Finite-Rate Elementary Chemical Reactions for Computing Diesel Combustion Process. *SAE Paper*, 2005-24-051, 2005.
- [23] O. Gicquel, N. Darabiha, and D. Thevenin. Laminar Premixed hydrogen/air counterflow flame simulations using flame propagation of ILDM with differential diffusion. *Proceedings of the Combustion Institute*, 28:pp. 1901–1908, 2000.
- [24] S. B. Pope. Computationally Efficient Implementation of Combustion Chemistry Using In-Situ Adaptive Tabulation. *Combustion Theory and Modelling*, 1:pp. 14–63, 1997.
- [25] B. Yang and S. B. Pope. Treating Chemistry in Combustion with Detailed Mechanisms - In Situ Adaptive Tabulation in Principal Directions - Premixed Combustion. *Combustion and Flame*, 112:pp. 85–112, 1998.
- [26] S. B. Pope, Z. Ren, L. Lu, V. Raman, and H. Pitsch. LES/PDF/ISAT Computations of Turbulent Premixed Flames. *Proceedings of the Summer Program*, 2004.
- [27] M. Embouazza, D. C. Haworth, and N. Darabiha. Implementation of Detailed Chemical Mechanisms Into Multidimensional Cfd Using in Situ Adaptive Tabulation: Application to HCCI Engines. *SAE Paper*, 2002-01-2773, 2002.
- [28] H. Hiroyasu, T. Kadota, and M. Arai. Development and Use of a Spray Combustion Model to Predict Diesel Engine Efficiency and Pollutant Emissions. Part 1: Combustion Modelling. *Bull JSME*, vol. 26(no. 214):pp. 569–575, 1983.
- [29] J. Nagle and R. F. Strickland Constable. Oxidation of Carbon between 1000–2000°C. *Proc. 5th Conf. on Carbon*, vol. 1:pp. 154–164, 1962.
- [30] J. B. Moss, C. D. Stewart, and K. J. Young. Modelling Soot Formation and Burnout in a High Temperature Laminar Diffusion Flame Burning Under Oxygen-Enriched Combustion. *Combustion and Flame*, vol. 101:pp. 491–500, 1995.
- [31] G. D'Errico and T. Lucchini. A Combustion Model with Reduced Kinetic Schemes for S.I. Engines Fuelled with Compressed Natural Gas. *SAE Paper*, 2005-01-1123, 2005.
- [32] T. Lucchini, G. D'Errico, H. Jasak, and Z. Tukovic. Automatic Mesh Motion with Topological Changes for Engine Simulation. *SAE Paper*, 2007-01-0170, 2007.
- [33] B. Stroustrup. *The C++ Programming Language*. Addison-Wesley, 3rd Edition, 1997.
- [34] *Programming Languages, C++*. ISO/IEC Standard 14822:1998, 1998.
- [35] H. Jasak. *FOAM CFD web site*, <http://www.foamcfd.org>. 2006.
- [36] L. M. Pickett and D. L. Siebers. Non-Sooting Low Flame Temperature Mixing-Controlled DI Diesel Combustion. *SAE Paper*, 2004-01-1399, 2004.
- [37] L. M. Pickett and D. L. Siebers. Soot in Diesel Fuel Jets: Effects of Ambient Temperature, Ambient Density and Injection Pressure. *Combustion and Flame*, 138:pp. 114–135, 2004.
- [38] P. F. Flynn, R. P. Durrett, G. L. Hunter, A. O. zur Loye, O. C. Akinyemi, J. E. Dec, and C. K. Westbrook. Diesel Combustion: An Integrated View Combining Laser Diagnostics, Chemical Kinetics and Empirical Validation. *SAE Paper*, 1999-01-0509, 1999.
- [39] A. Patel, S. C. Kong, and R. D. Reitz. Development and Validation of a Reduced Reaction Mechanism for HCCI Engine Simulations. *SAE Paper*, 2004-01-0558, 2004.
- [40] P. K. Senecal, E. Pomraning, and K. J. Richards. Multidimensional Modelling of Direct-Injection Diesel Spray Liquid Length and Flame Lift-off Length using CFD and Parallel Detailed Chemistry. *SAE Paper*, 2003-01-1043, 2003.
- [41] T. Cerri, A. Onorati, and E. Mattarelli. 1D Engine Simulation of a Small HSDI Turbocharged Engine Applying a Predictive Combustion Model. *Journal of Engineering for Gas Turbines and Power*, (To be published), 2007.
- [42] M.A. Singer and S.B. Pope. Exploiting ISAT to solve the equations of reacting flow. *Combustion Theory and Modelling*, Vol. 8:pp. 361–383, 2004.
- [43] A. Viggiano and V. Magi. A 2-D Investigation of n-Heptane Autoignition by Means of Direct Numerical Simulation. *Combustion and Flame*, 137:432–443, 2004.